Methane Diffusion Through Nanopore-Throat Geometry: A Molecular Dynamics Simulation Study

Runxuan Sun[1,2,3], Ke Xu[3]*, Tianjia Huang[3,4], and Dongxiao Zhang[3,5]*

[1]State Key Laboratory of Shale Oil and Gas Enrichment Mechanisms and Effective Development
[2]Sinopec Key Laboratory of Shale Oil/Gas Exploration and Production Technology
[3]Department of Energy and Resource Engineering, College of Engineering, Peking University
[4]Department of Petroleum Engineering, Texas A&M University
[5]Shenzhen Key Laboratory of Natural Gas Hydrates, Southern University of Science and Technology

Summary

Molecular diffusion dominates over pressure-driven convection as the major mass transport mechanism in nanoporous media with <10-nm pores, which is typical pore size for shale gas recovery. To study fluid behavior at this scale, molecular dynamics (MD) simulation has been widely applied. Nevertheless, classic capillary tube or slit models are of uniform geometry that miss the converging-diverging pore-throat feature, while more realistic models lose simplicity and generality.

In this work, we propose a novel geometric model that can reproduce the realistic converging-diverging structure in subsurface porous media without any additional complexity compared to classic slit or capillary models. In this pore-throat model, we are able to identify how nonuniform geometry affects the methane diffusion for both pure methane and for methane mixtures with water, carbon dioxide, and helium.

For a pure methane system, we demonstrate the fundamental impact of throat width on diffusion coefficient when the throat width is narrower than 20 Å and identify a critical throat width that determines whether methane can self-diffuse though the throat. This critical throat size is regulated by the energy barrier at the throat rather than by molecular size. We then introduce a semianalytical model to predict self-diffusion coefficient as a function of pressure, temperature, and throat width.

For mixtures, we observe the key impact of spatially nonuniform fluid distribution in determining diffusion. Water or carbon dioxide can locally concentrate at the throat, which reduces methane diffusivity, while helium prefers to stay in the pore body, which mildly enhances methane diffusivity. Specifically, although residual water reduces methane diffusion (26% reduction for 20% water molar fraction), it completely blocks the throat and thus prohibits pressure-driven methane convection. By comparison, the dominance of molecular diffusion over convection can be extended to larger pores in presence of residual water. It provides an explanation on shale gas production when connate water is expected to block the flow path.

Introduction

Porous media consisting of nanometer-scale pores (nanoporous media) in subsurface stratum, such as shale, play key roles in energy recovery and environmental engineering. In terms of shale gas recovery, shale provides storage space and migration paths for methane (Lee et al. 2016; Song et al. 2015). In terms of carbon capture, usage, and storage, shale acts as cap layers to inhibit carbon dioxide migration and leakage (Aljama and Wilcox 2017; Li et al. 2020; Skarmoutsos et al. 2013). Therefore, investigating gas transport mechanisms in nanoporous media is required (Guo et al. 2015; Jin and Firoozabadi 2015a).

Gas transports in porous media in two major ways: convection, driven by pressure gradient; and diffusion, driven by concentration gradient. Convection is commonly estimated by Darcy's law (Darcy 1856), written as $u = \frac{k}{\mu}\nabla P$, where u is Darcy velocity, k is permeability, ∇P is pressure gradient, and μ is viscosity. Diffusion is commonly estimated by Fick's law (Fick 1855), written as $J = -D * \nabla C$, where J is the molar diffusion flux, D is the diffusion coefficient, and ∇C is the molar concentration gradient. For conventional porous media, convection and convection-induced mechanical dispersion are generally presumed as the dominant mass transport mechanisms (Kasaeian et al. 2017). However, convection dramatically weakens with the decrease of pore size in quadratic order, while the diffusion is only mildly correlated to pore size. Therefore, dominance of convection may not still hold in shale that is mostly composed of nanopores (Jiao et al. 2014).

We estimate mass flux through Fick's law ($m_{\text{Fick}} = J * M$) and Darcy's law ($m_{\text{Darcy}} = u * \rho$), where M is the molecular weight, and ρ is the fluid density. A modified Péclet number can be defined as the ratio between fluxes driven by convection and by diffusion as $\text{Pe}^* = \frac{m_{\text{Darcy}}}{m_{\text{Fick}}} = \frac{k}{k_{\text{ref}}}$, where $k_{\text{ref}} = \frac{D * \mu}{P}$ can be defined as a reference permeability. If $\text{Pe}^* > 1$ ($k > k_{\text{ref}}$), convection dominates the mass transport; otherwise, diffusion dominates. Substituting typical subsurface environmental parameters (350 K, 20 MPa) (Wei et al. 2013) into its definition, we can estimate a typical reference permeability as $k_{\text{ref}} = 0.005$ md, corresponding to the pore diameter of 10 nm according to Kozeny-Carman estimation (Bear 1988). All shale gas reservoirs contain a significant portion of pores of less than 10 nm (Liehui et al. 2019), and many shale reservoirs are of lower permeability than 10^{-3} md (Shen et al. 2018). Diffusion can thus be a dominant mechanism of gas transport over convection in shale. Unfortunately, most investigations on gas transport through nanoporous media are still on convection (Kou et al. 2017; Pang et al. 2017).

*Corresponding author; email: kexu1989@pku.edu.cn; zhangdx@sustech.edu.cn

Original SPE manuscript received for review 25 May 2022. Revised manuscript received for review 3 August 2022. Paper (SPE 212289) peer approved 23 August 2022. Supplementary materials are available in support of this paper and have been published online under Supplementary Data at https://doi.org/10.2118/212289-PA. SPE is not responsible for the content or functionality of supplementary materials supplied by the authors.

Gas diffusion in nanoporous media is distinct from that in the macropores. Due to the smaller pore size compared to gas mean free path (Javadpour et al. 2007), continuum assumption is not available (Wu et al. 2015a). Molecular diffusion is through Knudsen diffusion (Phillip et al. 2006), where molecules frequently collide with the pore wall (Malek and Coppens 2003) and through surface diffusion, where molecules randomly hop between adsorption sites on the surface (Wu et al. 2015b). As a result, classic estimation of self-diffusion coefficient cannot be directly applied in nanoporous media.

It is challenging to conduct direct experimental measurements on gas diffusion in nanoporous materials (Lu et al. 2019) due to the limitation of time cost as well as high requirement of accuracy (Shilov et al. 2021). Consequently, MD method is prevalently adopted (Allen 2004). MD allows tracking of molecule trajectory to obtain the self-diffusion coefficient (Rapaport 2004). Based on molecule trajectory information, two methods can be applied to calculate the gas self-diffusivity in MD: Einstein's relation and the Green-Kubo relation. Einstein's relation uses mean square displacement (MSD) to observe the time, where the Green-Kubo relation uses the velocity autocorrelation function (Allen and Tildesley 2017; Frenkel and Smit 2001; Haile 1992).

A premise of conducting convincing MD simulations of mass transport in nanoporous structure is to construct an appropriate geometry model, which should represent key features of the investigated problem while balancing simplicity (for saving computational cost) and generality (for being representative). Commonly used geometries to represent nanopores include nanoslit and nanocylindrical tube. A slit-shape model can be constructed using graphene, kerogen, etc. as the wall, while the two walls are parallelly placed and separated by nanometer-scale space (Tesson and Firoozabadi 2018). Another commonly adopted geometry is capillary tube (Liu et al. 2005; Nanok et al. 2009). In capillary models of nanopore, carbon nanotube (CNT) is used extensively as the capillary material to simulate the organic nanopores (Chen et al. 2006; Jakobtorweihen et al. 2007; Skoulidas et al. 2002).

Regrettably, both the slit-shape models and capillary-shape models in MD studies miss the key feature of porous media—the converging-diverging porous geometry or "pore-throat structure." Pore-throat structure largely determines fluid transport in porous media of all scales (Skoulidas and Sholl 2003; Yan et al. 2017; Zhang et al. 2015). Throats are of local minimum of fluid conductivity so they quantize the porous media to be pore-network (Gensterblum et al. 2015). Throats are of local maximum of specific area so adsorption and capillary condensation preferentially emerge at throats (Yu et al. 2017). The pore-throat structure thus may result in nonuniform fluid distribution which can hardly be well reproduced in uniform capillary or slit models. Some researchers introduce kerogen to construct complex geometry, which can overcome this problem for specific cases (He et al. 2020); however, such construction of porous structure is very sensitive to kerogen molecular structure, thus lacks generality and is computationally costly. A simplified geometry model for MD that can represent pore-throat structure of nanoporous media is thus highly required.

In this proof-of-concept study, we introduce a representative and simple geometric model for MD simulation to study methane diffusion in pore-throat nanostructure:

1. First, we study the self-diffusion of pure methane in this nanopore-throat structure. We aim to quantify the effect of throat size, pressure, and temperature on self-diffusion coefficient and establish empirical model that takes pore-throat geometry into consideration.
2. Then, we extend the model to the mixtures of methane with carbon dioxide, water, and helium. We demonstrate how this geometry can simulate phenomena that cannot be reproduced in slit and capillary models, such as preferential adsorption and condensation at the throat.
3. Finally, we discuss some field-scale implications based on our MD observations, especially fundamental impact of nonuniform fluid distribution on methane transport mechanism in the presence of pore-throat structure.

Methods

MD simulation is used to study gas transport mechanisms at the nanoscale. All the parameters set for the MD simulation are based on the practical conditions of shale reservoir. A CNT model (Severson and Snurr 2007; Striolo et al. 2003) is built in visual MD software (Humphrey et al. 1996), material studio (MS) software (BIOVIA 2014) is used to calculate the molecular interactions, and large-scale atomic/molecular massively parallel simulator (or LAMMPS) software (Thompson et al. 2022) is used to simulate the MD. Open visualization tool (Stukowski 2009) and MATLAB® (MATLAB 2020) software are used to analyze the simulation results.

Geometry Setup and Boundary Conditions. A pore-throat structures model is built in the MD simulation box to study the gas self-diffusion in microscale. A fixed CNT with a radius of 10.16 Å is set in the center of the cubic rectangle box passing through the *z*-axis from the top to the bottom, as shown in **Fig. 1a**, to mimic fixed adsorbable organic matter in the nanoporous media. No gas molecules are to be set inside the CNT. The vacant space of simulation box in the *x*-axis is designed as the comparably large pore space with the length of 80 Å. The narrow space between the CNT and the up/bottom boundary along *y*-axis is to mimic the narrow pore throat between the nanotube and the mirrored nanotube in range of 6 to 60 Å. Molecules can be in the pore space and diffuse to other pores through the pore throat. Periodic boundaries are applied to all three axes of the simulation box, so particles can exit one end of the box and re-enter the other end (Rappe et al. 1992). According to this, a comprehensive porous media composed of pore-throat dual structures is formed in our simulation model as shown in **Fig. 1b**. The perspective view of simulation box is shown in **Fig. 1c**.

The space outside the CNT in the system can be classified into two regions—the "near-throat" region and the bulk region. The principle of classification is whether the molecule is directly affected by the nanotube in the system, which in simulation is decided by the global cutoff for molecular interactions. In this study, a distance of 14 Å is set as the global cutoff (Jones 1924).

The throat width can be regulated by the modification of the simulation box in the *y*-direction. There is thus no need to build a new nanotube model to conduct the simulation. Furthermore, even with the same unit cell structure, the change of nanotube diameters also affects the steric configuration of the nanotube unit structure, resulting in a different potential field. This deviation may give risk to the simulation results between case studies.

This introduced simulation model composed of pore-throat structures is closer to the real porous media than the traditional CNTs that molecules transport inside the tube of constant aperture, while no additional complexity is posed. The periodic boundary makes the MD more efficient to simulate porous media in a finite size, which saves a lot of computing capacity. The throat diameter can be simply regulated by modifying the simulation box size, with a fixed nanotube all the way through. In addition, there is no limit diameter for the throat.

Molecule Models. For the intermolecular potential, Lennard-Jones (L-J) potential is selected to describe the molecular interactions in the MD simulation. The L-J potential can be expressed as,

$$E_{lj} = 4\varepsilon\left[\left(\frac{\sigma}{r}\right)^{12} - \left(\frac{\sigma}{r}\right)^{6}\right], \qquad r < r_c, \tag{1}$$

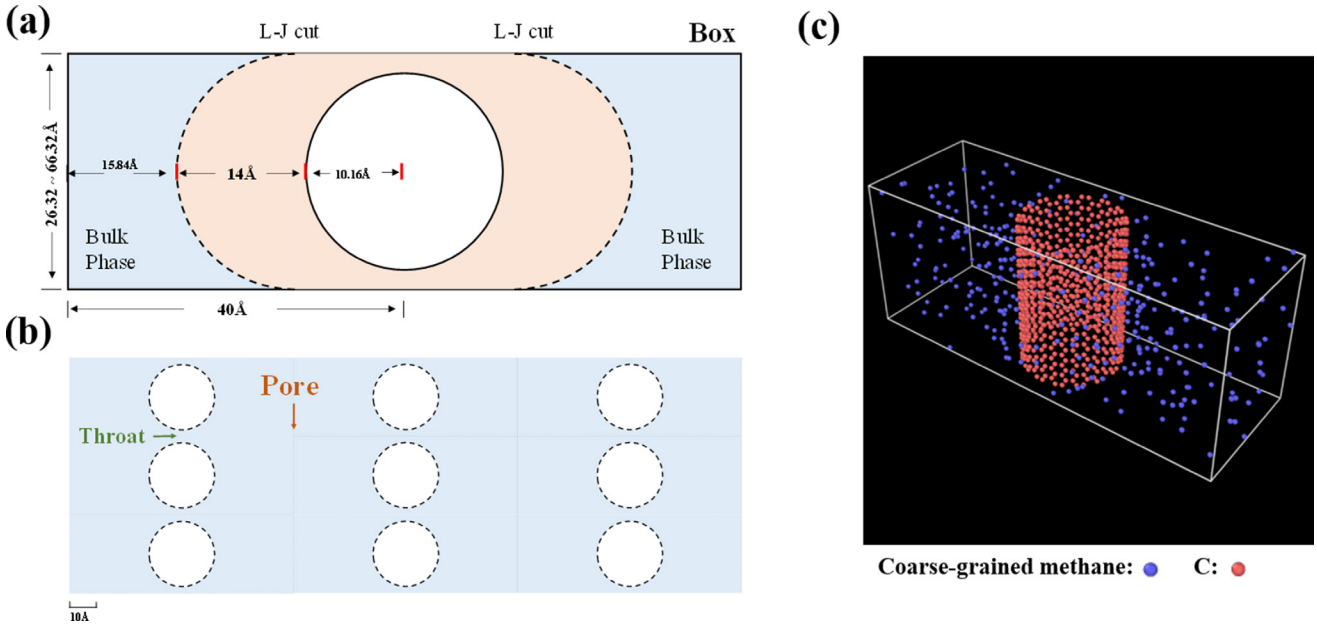

Fig. 1—Simulation model configurations: (a) top view of the simulation box, the orange zone indicates the molecules affected by the nanotube, and the blue zone indicates the molecules unaffected by the nanotube; (b) pore-throat dual structures porous media; and (c) the perspective view of MD simulation box.

where E_{lj} is the L-J pair potential, ε is the depth of the potential well (or "dispersion energy"), σ is the distance at which the particle-particle potential energy is zero (or "size of the particle"), r is the distance between two interacting particles, and r_c is the global cutoff. Columbian force can be expressed as,

$$E_c = \frac{C_{q_i q_j}}{\alpha r}, \qquad r < r_c, \tag{2}$$

where E_c is the Columbic force, C is an energy-conversion constant, q_i and q_j are the charges on the two atoms, and α is dielectric constant. Arithmetic mixing rules ($\sigma_{ij} = (\sigma_i + \sigma_j)/2$ and $\varepsilon_{ij} = \sqrt{(\varepsilon_i + \varepsilon_j)}$) are applied for the intermolecular pair potential calculation.

Columbian force is not considered for the coarse-grained methane molecule model, because methane is the nonpolar atom with no partial positive or negative charges. For the full-atom molecule model, both L-J pair potential and Columbian force is introduced to the system. The following combining rules are used to determine the cross parameters (Singh et al. 2009):

$$\sigma_{ij} = \frac{1}{2}(\sigma_i + \sigma_j), \tag{3}$$

$$\varepsilon_{ij} = (\varepsilon_i \varepsilon_j)^{\frac{1}{2}}, \tag{4}$$

$$\alpha_{ij} = (\alpha_i \alpha_j)^{\frac{1}{2}}. \tag{5}$$

Based on the literature and MS software, all the data used in this study is shown in **Table 1.**

The global cutoff is set as 14 Å, which is much larger than the adsorption layer thickness. Atom pair potentials are acquired from the literature: The TraPPE model is applied for the coarse grained methane molecules (Jin and Firoozabadi 2015b), and helium model is obtained by a steepest descent optimization routine (Talu and Myers 2001). For the full-atom model molecules, the pair potentials are outputs from the MS software under the CVFF and CLAYFF force field: CVFF force field is prevalently used in the organic and inorganic hybrid system (Lifson et al. 1979), and CLAYFF force field shows good promise in a wide adaption for molecular simulations of solid-liquid interfaces (Cygan et al. 2004). The applied molecule force field in this study has been verified by the literature, through accurately describing the physical phenomena of methane, water, and other substances (Kondori et al. 2019; Phan et al. 2012). All the L-J interactions are truncated at 1.4 nm, molecules under this truncation radius cannot interact with their image molecules. The CNT is fixed, and methane molecules are simulated in the canonical ensemble [number/volume/temperature (NVT) ensemble], where a Nose-Hoover thermostat is applied to control the temperature, and molecule motion is integrated by Verlet algorithm. In this ensemble, the simulation system can exchange energy with the heat bath to keep a fixed temperature, but the system total energy will change during the simulation process (Gibbs 1902).

Ensemble Setup. NVT ensemble is used to conduct the MD simulation in this study, for easy control and adjustment of the spatial structure of nanopores. With NVT ensemble, the pressure is calculated after certain molecules are inserted in fixed volume with fixed temperature.

To calculate the pressure, an imaginary wall is placed in the boundary of the x-direction, where methane molecules are all in the bulk phase. The hypothesis is that the methane colliding with the imaginary wall will be reflected at the same angle with the same velocity.

Atom Pair	ε/k (K)	σ (Å)	q (e)	References
C(graphene)	74.571	3.6170487995	0	MS
CH_4	148	3.73	0	Literature data*
$C(CH_4)$	80.6173	3.474505	–0.4	MS
$H(CH_4)$	19.14661	2.449971	0.1	MS
$C(CO_2)$	74.571	3.617049	0.5748	MS
$O(CO_2)$	114.8797	2.859785	–0.28774	MS
$O(H_2O)$	78.30782	3.16552	–0.82	MS
$H(H_2O)$	0	0	0.41	MS
He	10.9	2.64	0	Literature data†

*Jin and Firoozabadi (2015b).
†Talu and Myers (2001).

Table 1—Lennard-Jones (L-J) 12-6 potential parameters for adsorption in graphene.

Under these conditions, the changes of momentum, which are impulses, are summarized for methane molecules passing through one direction in the x-axis to calculate the pressure (Blundell and Blundell 2010), as:

$$P = \sum_{n=1}^{N} 2mv\cos\theta, \tag{6}$$

where P is the calculated system pressure, n is the methane molecule number, N is the total amount of methane molecules which pass through one direction boundary in the x-axis, m is the methane molecule weight, v is the methane velocity, and θ is the normal angle for the imaginary wall.

Every time we set a molecule number, the resulting pressure using NVT ensemble can be calculated. If the resulting pressure is higher (or lower) than the wanted pressure, we reduce (or increase) the number of molecules and conduct next try. Within a few iterations, we can find the N for the wanted P, so further sensitivity analysis case studies can be carried out.

Numerical Experiment Procedures. The simulation workflow can be divided into three steps. First, the methane molecules are inserted randomly into the simulation box outside the CNT and relaxed for 100 picoseconds (ps) to balance the system. Second, an extra 50-ps simulation is conducted to quantify the system pressure. If the pressure is not acceptable (>1 MPa larger or smaller than the target pressure), the first step will be replayed with increased or reduced methane molecule numbers. After an acceptable pressure is achieved, the methane diffusion coefficient or molecule flux is measured in 1,000 ps.

To verify that the equilibrium has been reached after 100-ps relaxation, the system total energy and molecule number difference between the left and right sides are calculated. The result is shown in Fig. S-1 in the Supplementary Material, system total kinetic energy variation is less than 4% and the mean difference of methane molecule number is close to zero, indicating a good system equilibrium.

Data Acquirement. To count for the number of methane molecules flowing through the throat, an imaginary wall is placed in the center of the throat in the y-z direction. If the methane molecule flows through the imaginary wall in the x-direction, then the counted number of methane molecules passing through the wall is added or deducted by one. The timestep used in this simulation is 1 femtosecond. Using the counted number of methane molecules divided by area of imaginary wall and simulation time, the absolute molecule flux can be calculated.

As the throat is specifically conducting transport at the x-axis, we study the diffusion coefficient in the x-direction, where gas must pass through a sequence of throats and pore bodies to diffuse through porous media. There are mainly two methods to calculate the self-diffusion coefficient, which are Einstein's relation (Ma et al. 2017) and the Green-Kubo relation (Mouas et al. 2012). Einstein's relation integrates the differentiation of MSD with respect to time. In the Green-Kubo relation, the diffusion property is calculated as an integral of the velocity autocorrelation function with respect to time. Considering the isotropic system simulated in this study, the simple Einstein's relation is applied to calculate the self-diffusion coefficient (Miller 1924), shown as:

$$\left\langle \Delta x^2\left(t\right)\right\rangle = 2D_x t, \tag{7}$$

where $\left\langle \Delta x^2\left(t\right)\right\rangle$ is the ensemble of mean squared displacement inthe x-direction during simulation time, D_x is the parallel self-diffusion in the x-direction, and t is the simulation time.

Self-Diffusion of Pure Methane

We first demonstrate the applicability of this model in studying pure methane self-diffusion. The coarse-grained method is prevalently used in MD simulations (Jacobson and Molinero 2010; Rudd and Broughton 1998), especially for the highly symmetrical structured methane (Sobolewski et al. 2009). Due to the relatively isotropic nature of methane molecules, the coarse-grained method is applied in this study to save computational resources.

Critical Throat Width. Methane self-diffusion in geometries of different throat widths is studied under the same condition (350 K, 20 MPa). **Fig. 2a** shows the absolute molecular flux (total frequency of passing the throat over the throat area, regardless of its direction).

A critical throat width of 6.3 Å for fluid self-diffusion through the porous media is identified, below which no methane molecule transports through the throat. We note that it is larger than the diameter of methane molecules (4.14 Å), which indicates that whether a molecule

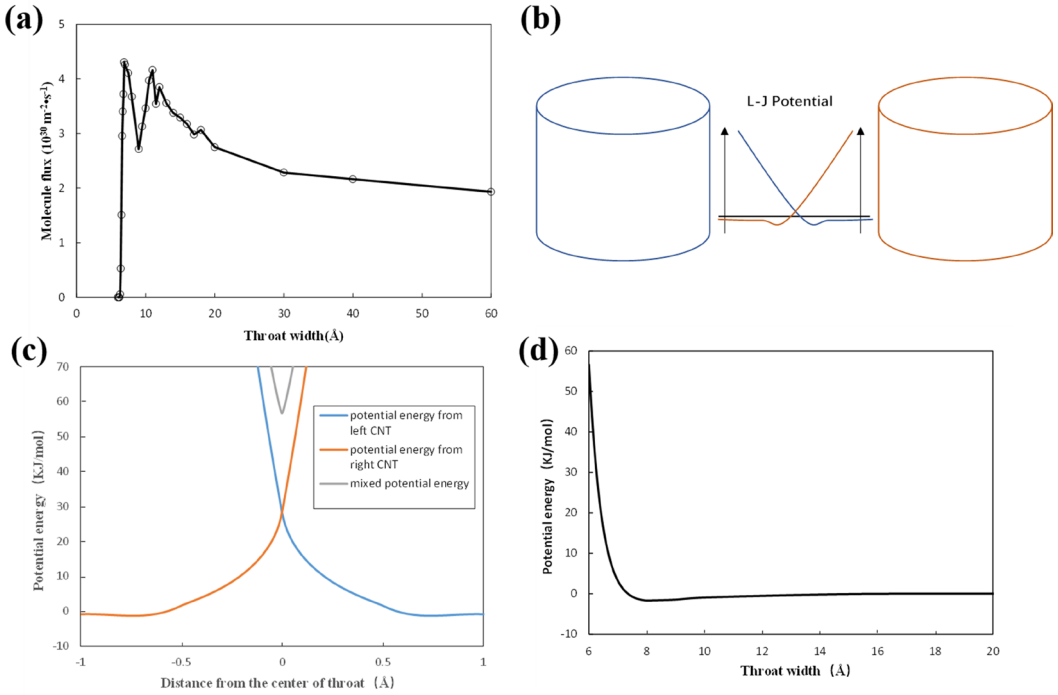

Fig. 2—Methane critical throat width analysis in the pore-throat structure model. (a) Methane molecule flow through throat. (b) Schematic diagram of L-J potential energy. (c) Potential energy distribution in 6-Å throat. Red lines represent the right CNT, blue lines represent the left CNT, and gray line represents the mixed potential energy. (d) Potential barrier energy of the throat in different throat width.

can pass through a throat is determined not only by molecular size. To better analyze this phenomenon, we calculate the potential energy between methane and graphene in the throat.

Fig. 2b shows a schematic diagram of the throat formed by two CNTs. The potential energy field overlaps together, which forms an energy barrier (or well) in the center of the throat (**Fig. 2c**). If the height of barrier or depth of the well is higher than the molecular kinetic energy, the molecules would be repelled from or trapped inside it, thus preventing the molecules flux through the throat. Only if the kinetic energy is higher than the potential barrier or well, might methane molecules have a chance to move through the throat. The kinetic energy (ke) of methane molecules can be estimated by $ke = 3/2 \times kT$, where k is the Boltzmann constant and T is the system temperature. As shown in **Fig. 2d**, under the simulation conditions, the kinetic energy for methane molecule is about 4.5 kJ/mol, indicating a critical throat width of around 6.9 Å. The simulated critical throat width for methane to move through is comparable to the thermodynamic calculation results. It rationalizes our observation of this critical throat width to allow molecular flux.

In summary, a critical throat width exists in porous media, which is determined by the ratio of potential barrier over molecular kinetic energy, rather than by molecular diameter.

Self-Diffusion Coefficient. We calculate the evolution of MSD with time for methane molecules under different throat widths, pressures, and temperatures. To eliminate the deformation of spatial structure induced by the change of pore-throat relation, a steric configuration parameter θ is introduced as $\theta = \frac{L_t}{L_t + L_n}$, where L_t is the width of the throat and L_n is the length of nanotube diameter. The simulation results of MSD/θ at 350 K and 20 MPa are shown in **Fig. 3a.**

As is clearly shown in **Fig. 3a**, the evolution curves of methane molecule MSD for all throat widths well overlap at the beginning while hey deviate significantly when time is larger than 200 ps. We note that the moment of deviation is about (60 Å)^2, which well corresponds to the size of the pore body. It indicates that the self-diffusion of methane in a single pore is captured in an earlier timestep. And in the late periods, the self-diffusion capacity of methane is characterized to transport through one pore unit and another (i.e., nanoporous media).

Specifically, the MSD when throat width of 6 Å (blue line) reaches the plateau is at about 200 ps. The height of this plateau is approximately the maximum MSD inside a single pore, showing that molecules cannot pass through the throat, which echoes the zero molecular flux through throat at this throat width. For a throat wider than the critical width, an approximately proportional correlation between MSD and time is captured after 200 ps, which agrees with the Einstein equation. Larger throat size results in larger MSD. We can thus calculate the self-diffusion coefficient in the following simulation analysis using linear fitting of data after 200 ps.

Under the temperature of 350 K and pressure of 20 MPa, we calculate methane self-diffusion coefficients for throat width ranging from 0 to 60 Å, as shown in **Fig. 3b**. With the increase of the width of the throat, the methane self-diffusion coefficient increases first with fluctuation and reaches a maximum when the throat width is approximately 18 Å and then becomes relatively stable. MSD data for all numerical experiments are shown in Figs. S-2 through S-4 and Tables S-1 through S-14 in the Supplementary Material.

We further quantify the self-diffusion coefficient of methane under pressures of 10, 30, and 50 MPa with different throat widths from 6 to 60 Å at 350 K, as shown in **Fig. 4a.** The methane self-diffusion coefficients for high pressures (20, 30, and 50 MPa) share a similar trend. As the throat width increases, the methane self-diffusion coefficient increases relatively dramatically until reaching the peak at about 18 Å. Then, the methane self-diffusion coefficient tends to be constant after a small reduction. However, the maximum diffusion coefficient does not sit at 18 at 10 MPa, although a local peak value does sit there. In the Supplementary Material, we show our hypothesis that this peak at 18 Å for high pressure is highly correlated to the adsorption layers in Fig. S-5.

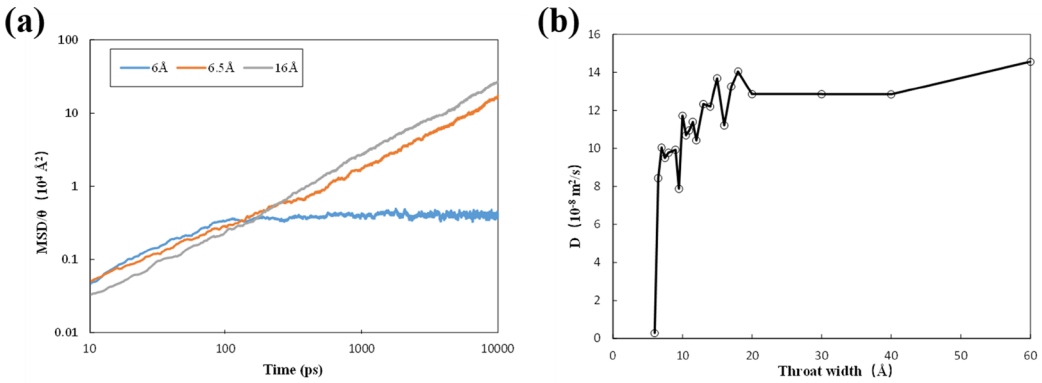

Fig. 3—(a)Calculated MSD/*θ* vs. simulation time. (b) Revised methane self-diffusion coefficient under 350 K, 20 MPa.

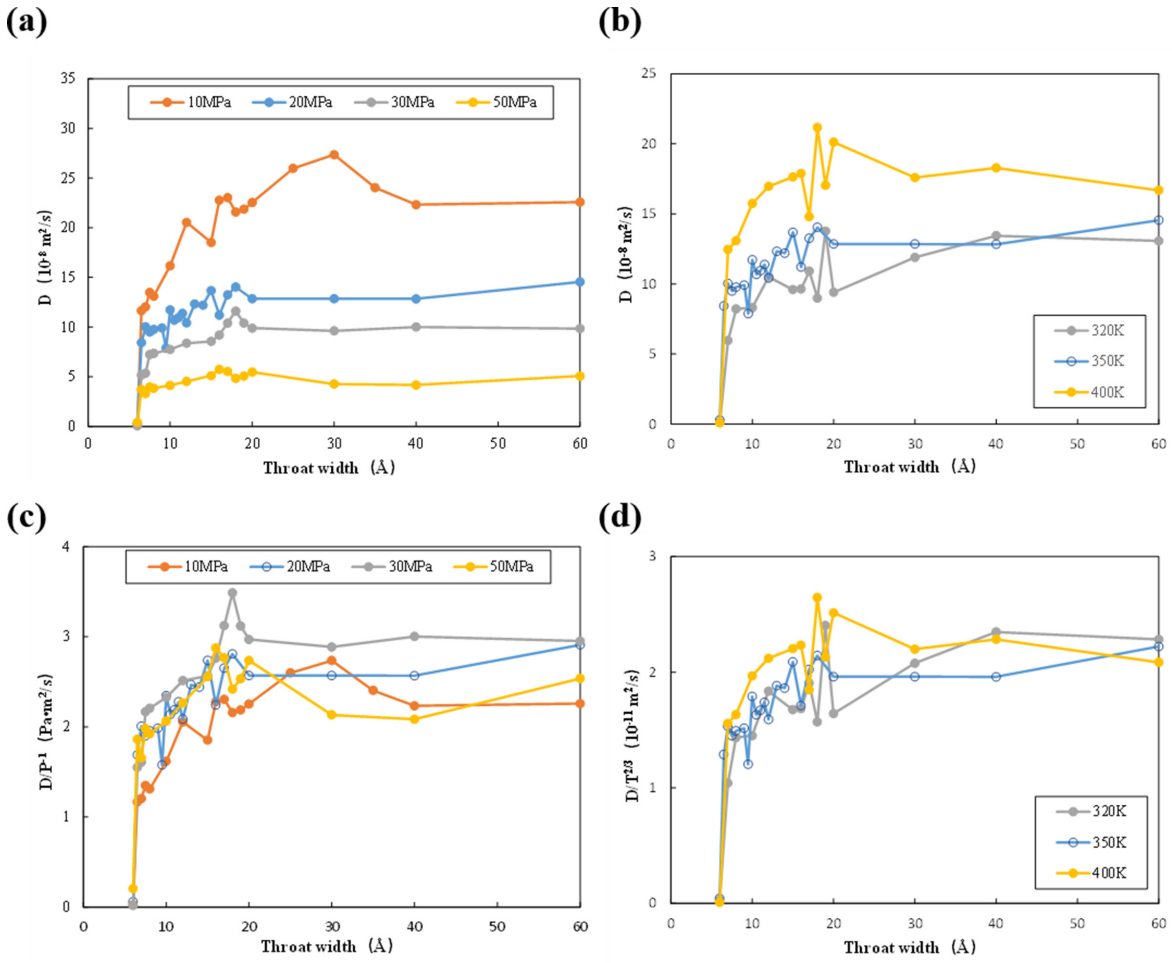

Fig. 4—Methane self-diffusion coefficients under different throat width, pressure, and temperature: (a) methane self-diffusion coefficient vs. throat width under different pressures; (b) methane self-diffusion coefficient vs. throat width under different temperatures; (c) methane self-diffusion coefficients under different pressures overlap after being rescaled by *P*; and (d) methane self-diffusion coefficients under different temperatures overlap after being rescaled by $T^{3/2}$.

To investigate the effect of temperature, a lower temperature of 320 K and a higher temperature of 400 K are simulated under the pressure of 20 MPa. The results of methane self-diffusion are shown in **Fig. 4b**. Statistically, higher temperature correlates to larger methane self-diffusion coefficient.

Prediction of Methane Self-Diffusion Coefficient in the Pore-Throat Structure. For bulk gas, it has been discovered that self-diffusion coefficient is inversely proportional to the pressure and is proportional to 3/2 power to the temperature (i.e., D/P^{-1} is a constant at a fixed temperature and $D/T^{3/2}$ is a constant at fixed pressure) (Blundell and Blundell 2010). We thus test whether these scaling arguments still work for methane self-diffusion.

We plot D/P^{-1} vs. throat width for all data at 350 K as shown in **Fig. 4c** and plot $D/T^{3/2}$ vs. throat width for all data at 20 MPa as shown in **Fig. 4d**. We find that these curves well overlap, although the diffusion is not for bulk fluid.

Data show that throat width significantly affects the value of D/P^{-1} and $D/T^{3/2}$. It increases rapidly when throat width increases from the critical width to 20 Å. For throat width larger than 20 Å, D/P^{-1} and $D/T^{3/2}$ do not change much with throat width anymore.

Accordingly, we propose a semianalytical model to predict gas self-diffusion coefficient that takes pressure, temperature, and throat width ino consideration, as

$$D = a\frac{T^{3/2}}{P}\left\{1 - \exp\left[b\left(w_0 - w\right)\right]\right\}, \tag{8}$$

where a is a parameter so that $a\frac{T^{3/2}}{P}$ equals to self-diffusion coefficient in bulk, w is the throat width, and w_0 (6.3 Å in this study as we measured) is the critical throat width to allow gas diffusion passing through. We note that only b is a fitting parameter. **Fig. 5** shows that Eq. 8 fits the numerical simulation data well, where b is determined as 0.7. We thus provide a bridge to the knowledge gap of diffusion coefficient through nanoconfinement between 0 to 5 nm.

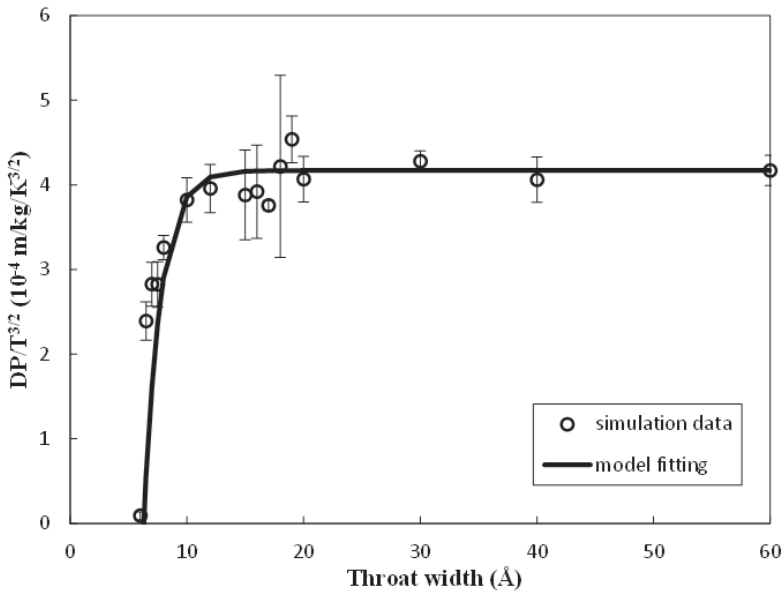

Fig. 5—Comparison between numerical simulation of methane self-diffusion coefficients in the pore-throat geometry at different pressures, temperatures, and throat widths.

Diffusion of Carbon Dioxide, Water, Helium, and Their Mixture with Methane

In this section, we extended the application beyond pure methane to methane mixtures with other components. The aim of this section is to show how this pore-throat geometry can well reproduce the uneven fluid distribution and how this uneven fluid distribution may change methane migration mechanisms.

Carbon dioxide and water are chosen for demonstration as they are the two most typical components that may emerge in a methane reservoir (Heller and Zoback 2014; Ross and Marc Bustin 2009). In addition, helium is also investigated due to its high economic value and its emergence in methane reservoir (Li et al. 2021).

Given the anisotropic nature of carbon dioxide and water molecules, full-atom models (rather than coarse-grained models) are applied in this section as introduced in Molecule Models. To verify the coincidence of full-atom model and coarse-grained model, the pure methane self-diffusion in the introduced pore-throat structure is simulated with the throat width of 10 Å and temperature of 350 K. Three hundred methane molecules are simulated in the simulation box; the system pressure is calculated as 16 and 14 MPa for the full-atom model and the coarse-grained model, respectively. The revised self-diffusion coefficient for the full-atom model is 1.2427×10^{-7} m^2/s and for the coarse-grained model is 1.3591×10^{-7} m^2/s. The difference is thus less than 10% between the full-atom model and the coarse-grained model.

Critical Throat Width for Pure Carbon Dioxide, Water, and Helium. We first test the diffusion of pure carbon dioxide, water, and helium in the pore-throat model. Corresponding images are as shown in **Figs. 6a through 6c.** Different from methane that cannot pass through a throat narrower than 6.3 Å (verified with full-atom model as shown in Fig. S-6 in the Supplemental Material), carbon dioxide, water, and helium molecules can all pass through throats as narrow as 6 Å.

We note that molecule diameters of carbon dioxide and water are 3.5–5.1 and 4 Å, which are slightly larger than that of the methane, so their capability to pass through smaller throats than methane needs rationalization. We attribute the smaller critical throat width for carbon dioxide and water to their different configuration from methane's. Methane has a relatively isotropic 3D configuration while carbon dioxide and water are highly anisotropic with 1D or 2D configuration. Therefore, by aligning with the throat direction, the potential energy barrier at the center of the throat can be significantly reduced, as shown in **Fig. 6d**.

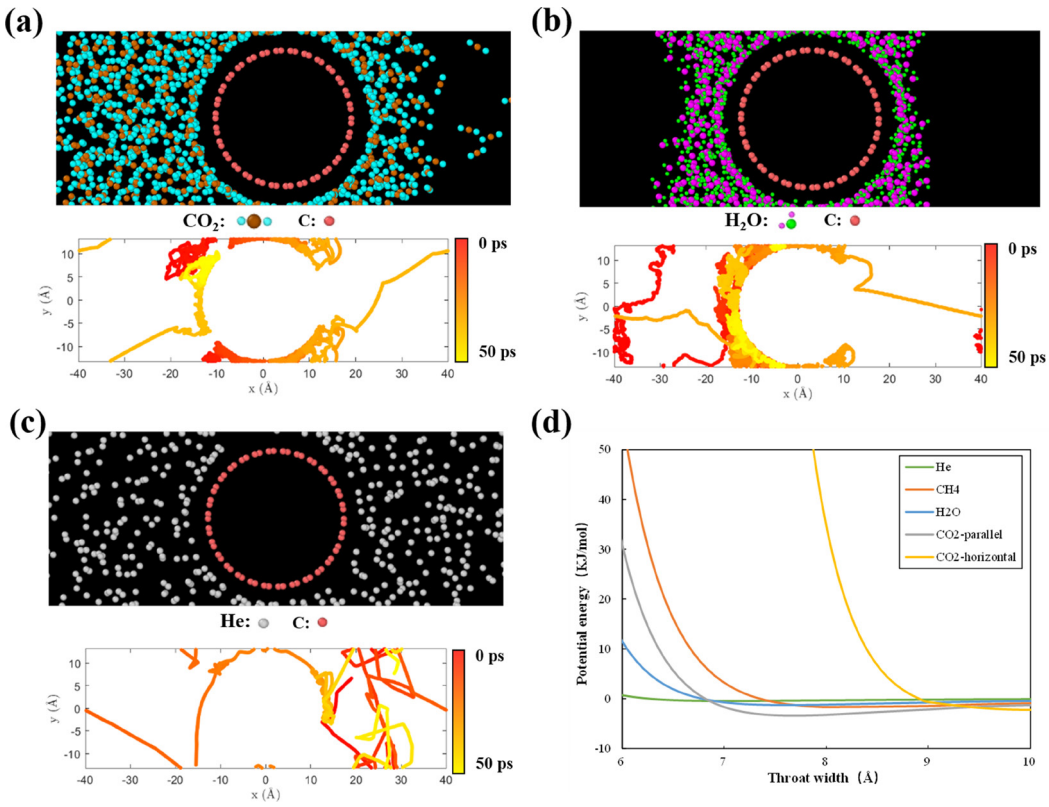

Fig. 6—Pure carbon dioxide, water, and helium simulation results. (a) Top view of pure carbon dioxide simulation box and the trajectory of one carbon dioxide molecule diffusing through the 6-Å throat in pure carbon dioxide system. Cyan and brown particles represent the carbon and oxygen of carbon dioxide. (b) Top view of pure water simulation box and the trajectory of one water molecule diffusing through the 6-Å throat in pure water system; purple and green particles represent the oxygen and hydrogen of water. (c) Top view of pure helium simulation box and the trajectory of one helium molecule diffusing through the 6-Å throat in pure helium system; gray particles represent the helium. (d) Energy barrier of the throat in different throat width.

Methane Diffusion in Mixtures. We simulate the behaviors of methane-water mixture **(Fig. 7a),** methane-carbon dioxide mixture (**Fig. 7b**), and methane-helium mixture (**Fig. 7c**) in the nanopore-throat unit. In this demonstrative simulation, three mixtures are of the same molar ratio (the molar ratio between methane and carbon dioxide, water, or helium is 4:1), under the same reservoir conditions (350 K and 20 MPa), in a pore-throat geometry with throat width of 20 Å. Given the complexity of the mixture system, the relaxation time is extended to 500 ps. The simulation results of methane diffusion coefficients, their change compared to pure methane, and species ratio at different regions are shown in **Table 2.**

	Methane Diffusion Coefficient (m^2/s)	Methane Diffusion Coefficient Change	Methane Ratio in Throat	Methane Ratio in Pore
Methane-carbon dioxide mixture	1.11×10^{-7}	–26%	2.8:1	7.8:1
Methane-water mixture	1.14×10^{-7}	–24%	2.4:1	21.1:1
Methane-helium mixture	1.64×10^{-7}	+9%	38.6:1	1.8:1

Table 2—Methane mixture simulation results.

Methane diffusion coefficients in these mixtures are calculated as 1.11×10^{-7} m^2/s for carbon dioxide-methane mixture, 1.14×10^{-7} m^2/s for in water-methane mixture, and 1.64×10^{-7} m^2/s helium-methane mixture. As a reference, the pure methane self-diffusion coefficient at same condition is calculated by full-atom model as 1.50×10^{-7} m^2/s. The results show that the existence of 20% carbon dioxide, water, and helium change the diffusion coefficient of methane by −26, −24, and +9%.

From the observation of molecular spatial distribution **(Fig. 7)**, we attribute this change of diffusion coefficient to the preferential adsorption of specific component in throat. We calculate the molar ratio of the mixture in the throat region (green part) and in the bulk region (orange part), as shown in **Fig. 7d**. For methane-carbon dioxide mixture, the molar ratio between methane and carbon dioxide in the throat region is 2.8:1 and in the pore region is 7.8:1. For methane-water mixture, the molar ratio between methane and water in the throat region is 2.4:1 and in the pore region is 21:1. In both cases, the molar ratio of methane in the near-throat region is much lower than the average molar ratio and that in the bulk region is much higher than the average molar ratio. Specifically, the distribution of water shows clear capillary condensation behavior (Yamashita et al. 2017). This preferential adsorption of carbon dioxide and water provides additional obstacles for methane to diffuse through the throat. In contrast, for helium-methane mixture, the molar ratio between methane and helium in the throat region is 38.6:1 and in the pore region is 1.8:1, showing that methane is preferential to adsorb in the throat. The

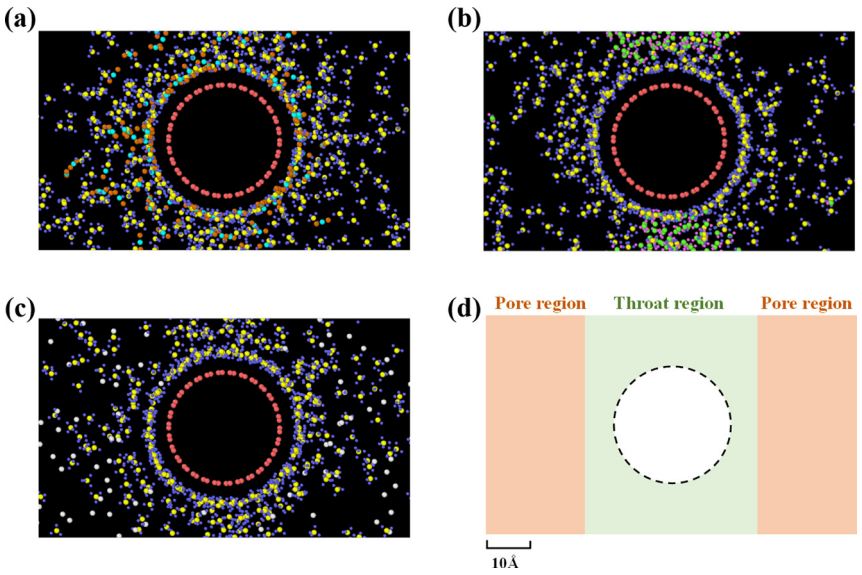

Fig. 7—Top view of methane mixture simulation results: (a) carbon dioxide-methane mixture simulation in the 20-Å throat, where cyan and brown particles represent carbon and oxygen of carbon dioxide molecules, and yellow and blue particles indicate carbon and hydrogen of methane molecules; (b) water-methane mixture forms the condensed water phase in the 20-Å throat, where purple and green particles represent oxygen and hydrogen of water molecules, and yellow and blue particles represent carbon and hydrogen of methane molecules; (c) helium-methane mixture simulated in the 20- Å throat, where gray particles represent helium molecules, and yellow and blue particles represent carbon and hydrogen of methane molecules; and (d) schematic diagram of molar ratio distribution division of different regions.

molar ratio of methane in the near-throat region is much higher than the average molar ratio, resulting in increased frequency to path through the throat and therefore higher diffusion coefficient.

We note that this preferential adsorption cannot be reproduced in traditional slit or capillarity models, due to the absence of converging-diverging geometry. It thus highlights the advantage of our new pore-throat model in future MD investigations of transport phenomena in porous media.

Impact of Residual Water on Methane Diffusion. As shown in **Fig. 7b** and **Table 2**, water prefers to distribute at the throat when it coexists with methane. This is like the capillary condensation that prefers high specific-area region, which cannot be reproduced by traditional slit or capillarity models. We then look into how residual water content influences methane diffusion.

We simulate water-methane mixture under the condition of 350 K, 20 MPa, with the throat width of 20 Å. We vary the water molar fraction from 0 to 90%. Methane diffusion coefficients at different water contents are demonstrated in **Fig. 8A.** Not surprisingly, methane diffusion coefficient decreases with increased water content. From pure methane to 50% water, the methane diffusion coefficient reduces by approximately 60%.

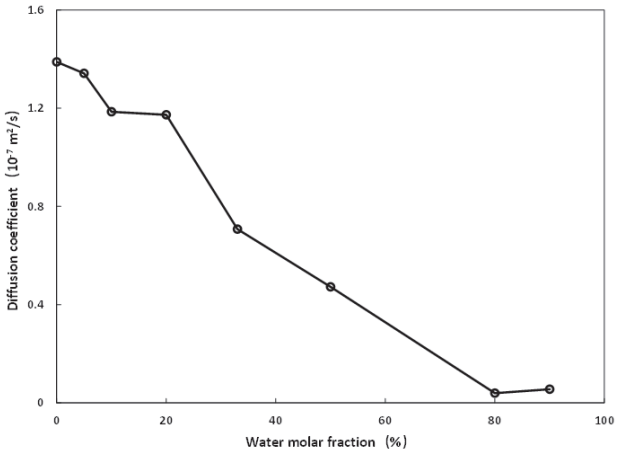

Fig. 8—Methane diffusion coefficients in methane-water mixtures of different water molar fractions.

Although diffusion is suppressed by residual water in pore-throat geometry, the reduced diffusion coefficient is still at the same order of magnitude as pure methane. In contrast, the residual water completely blocks the hydrodynamic flow path. Any pressure-driven convection needs to overcome the capillary pressure barrier to be initiated, which in this case is approximately ~10^7 Pa per pore, which is far

beyond realistic practice. As a consequence, the dominance of molecular diffusion over pressure-driven convection is largely enhanced when residual water exists.

Implications

1. Single-component simulations show that a geometric criterion exists for methene and other gas to mobilize in nanoporous media, which is determined by whether energy barrier dominates over molecular kinetic energy rather than by the size of molecules. It would help us to analyze the potential in-situ availability of methane in tight organic matters after resolving the geometry.
2. Preferential distribution on throat largely determines the diffusion of different components in mixture. In presence of other components (water, carbon dioxide, etc.) that preferentially adsorb at throat, methane diffusion is suppressed. Therefore, a "relative diffusion coefficient" idea may be necessary as an analog to relative permeability concepts to depict multicomponent diffusion in nanoporous media. In carbon dioxide-based shale gas enhanced oil recovery practices (Ebrahim and Akkutlu 2014; Louk et al. 2017; Xiang and Elsworth 2015; Xu et al. 2017), this reduction of methane mobility should be considered.
3. Another interesting implication is that methane can still be recoverable when connate water exists that forms liquid bridges, even if the liquid bridge disables pressure-driven flow. That is because connate water bridge at the throat still allows molecular diffusion, although the diffusion coefficient is mildly reduced. Thus, the emergence of connate water results in dominance of diffusion over convection in even larger pores, which makes the transport of methane still possible when pressure-driven flow is blocked.

Conclusion

A simple and representative pore-throat model is introduced in MD simulation to study gas diffusion in nanoporous media. It provides adjustable converging-diverging geometry that is a key feature to differentiate porous media from uniform geometric confinements while requiring no additional computational complexity than traditional slit or capillary models.

We first study pure methane self-diffusion in nanoporous media under subsurface conditions. A critical throat width about 6.3 Å is identified, below which methane molecules cannot diffuse through the throat. This critical size is theoretically rationalized by comparing energy barrier at the throat and molecular kinetic energy. We show that $DP/T^{3/2}$ throat width curves for all investigated pressures and temperatures overlap well, which are highly sensitive to throat width when throat is narrower than 20 Å. We accordingly propose a semi-analytical model to predict D as a function of T, P, and throat width.

We further generalize this model to carbon dioxide, water, and helium as well as their mixtures with methane. We show that the presence of carbon dioxide and water significantly weakens the diffusion of methane through the throat due to the preferential adsorption or capillary condensation of carbon dioxide and water at the throat that provides additional resistance to methane. In contrast, helium mildly enhances the diffusion of methane through the throat, as helium prefers to stay in the pore body and concentrates methane near the throat. The impact of water molar fraction on methane diffusion coefficient is further quantified. The discovery of spatially nonuniform molecule distribution between throat and pore body highlights the physical feasibility of our model in MD investigation of mass transport in nanoporous media.

We show the following implications that may be of significance for field applications:

- A geometric criterion of throat width exists for methane to mobilize in nanoporous media, which determines in-situ availability of shale gas.
- Methane diffusion is suppressed in the presence of other components that preferentially adsorb at the throat, which brings new questions for carbon dioxide-based shale gas enhanced oil recovery.
- Connate water may completely disable pressure-driven flow while still allowing molecular diffusion, which may rationalize the shale gas production at high water content where water blockage is expected.

Data Availability Statement

MD simulation model is built up through the visual MD (Humphrey et al. 1996), http://www.ks.uiuc.edu/Research/vmd, and MS 7.0 software (BIOVIA, 2014), http://www.nsccsz.cn/nsccsz2020/index.shtml. LAMMPS software is used to simulate the MD model (Thompson et al. 2022), https://www.lammps.org/. MD simulation figures are made with open visualization tool software (Stukowski 2009), https://www.ovito.org/. MATLAB (R2020b) is used to analyze the simulation output data (MATLAB 2020), https://www.mathworks.com/. The data presented in this study are included in the Supplemenatary Materials. Detailed information about our MD simulation data for the figures are available online, Figshare, https://doi.org/10.6084/m9.figshare.19753582. Translation available via browser plug-in.

Acknowledgment

This work was supported by the Sinopec Petroleum Exploration and Production Research Institute (33550000-21-ZC0613-0314). Their support is appreciated. We are especially indebted to Prof. Mohan Chen and Dr. Yinan Chen from Peking University and Dr. Tianhao Wu from Southern University of Science and Technology for the assistance in modifying the MD simulation scheme. We are grateful to the High-performance Computing Center of the National Supercomputer Center in Shenzhen.

References

Aljama, H. and Wilcox, J. 2017. Microscopic Diffusion of CO_2 in Clay Nanopores. *Chem Phys Lett* **677**: 162–166. https://doi.org/10.1016/j.cplett.2017.04.012.

Allen, M. P. 2004. Introduction to Molecular Dynamics Simulation. In *Computational Soft Matter: From Synthetic Polymers to Proteins*, Vol. 23, 1–28. Jülich, Germany: John von Neumann Institute for Computing.

Allen, M. P. and Tildesley, D. J. 2017. *Computer Simulation of Liquids*. Oxford, UK: Oxford University Press.

Bear, J. 1988. *Dynamics of Fluids in Porous Media*. New York, New York, USA: Dover Publications.

BIOVIA, D. S. 2014. Material Studio 7.0 Software. San Diego, California, USA: Dassault Systèmes.

Blundell, S. J. and Blundell, K. M. 2010. *Concepts in Thermal Physics*. Oxford, UK: Oxford University Press. https://doi.org/10.1093/acprof:oso/9780199562091.001.0001.

Chen, H., Johnson, J. K., and Sholl, D. S. 2006. Transport Diffusion of Gases Is Rapid in Flexible Carbon Nanotubes. *J Phys Chem B* **110** (5): 1971–1975. https://doi.org/10.1021/jp056911i.

Cygan, R. T., Liang, J. J., and Kalinichev, A. G. 2004. Molecular Models of Hydroxide, Oxyhydroxide, and Clay Phases and the Development of a General Force Field. *J Phys Chem B* **108** (4): 1255–1266. https://doi.org/10.1021/jp0363287.

Darcy, H. 1856. *Les Fontaines Publiques de La Ville de Dijon: Exposition et Application*, 305–310. Paris, France: Dalmont.

Ebrahim, F. and Akkutlu, I. Y. 2014. Multi-Component Gas Transport and Adsorption Effects during CO_2 Injection and Enhanced Shale Gas Recovery. *Int J Coal Geol* **123**: 52–61. https://doi.org/10.1016/j.coal.2013.07.021.

Fick, A. 1855. V. On Liquid Diffusion. *Lond Edinb Dublin Philos Mag J Sci* **10** (63): 30–39. https://doi.org/10.1080/14786445508641925.

Frenkel, D. and Smit, B. 2001. *Understanding Molecular Simulation: From Algorithms to Applications*. Amsterdam, The Netherlands: Elsevier.

Gensterblum, Y., Ghanizadeh, A., Cuss, R. J. et al. 2015. Gas Transport and Storage Capacity in Shale Gas Reservoirs–A Review Part A: Transport Processes. *J Unconv Oil Gas Resour* **12**: 87–122. https://doi.org/10.1016/j.juogr.2015.08.001.

Gibbs, J. W. 1902. *Elementary Principles in Statistical Mechanics Developed with Especial Reference to the Rational Foundation of Thermodynamics*. New York, USA: Scribner's Sons. https://doi.org/10.5962/bhl.title.32624.

Guo, C., Xu, J., Wu, K. et al. 2015. Study on Gas Flow through Nano Pores of Shale Gas Reservoirs. *Fuel* **143**: 107–117. https://doi.org/10.1016/j.fuel.2014.11.032.

Haile, J. M. 1992. *Molecular Dynamics Simulation: Elementary Methods*. Hoboken, New Jersey, USA: John Wiley & Sons, Inc.

He, J., Ju, Y., Lammers, L. et al. 2020. Tortuosity of Kerogen Pore Structure to Gas Diffusion at Molecular- and Nano-Scales: A Molecular Dynamics Simulation. *Chem Eng Sci* **215**: 115460. https://doi.org/10.1016/j.ces.2019.115460.

Heller, R. and Zoback, M. 2014. Adsorption of Methane and Carbon Dioxide on Gas Shale and Pure Mineral Samples. *J Unconv Oil Gas Resour* **8**: 14–24. https://doi.org/10.1016/j.juogr.2014.06.001.

Humphrey, W., Dalke, A., and Schulten, K. 1996. VMD: Visual Molecular Dynamics. *J Mol Graph* **14** (1): 33–38. https://doi.org/10.1016/0263-7855(96)00018-5.

Jacobson, L. C. and Molinero, V. 2010. A Methane-Water Model for Coarse-Grained Simulations of Solutions and Clathrate Hydrates. *J Phys Chem B* **114** (21): 7302–7311. https://doi.org/10.1021/jp1013576.

Jakobtorweihen, S., Lowe, C. P., Keil, F. J. et al. 2007. Diffusion of Chain Molecules and Mixtures in Carbon Nanotubes: The Effect of Host Lattice Flexibility and Theory of Diffusion in the Knudsen Regime. *J Chem Phys* **127** (2). https://doi.org/10.1063/1.2753477.

Javadpour, F., Fisher, D., and Unsworth, M. 2007. Nanoscale Gas Flow in Shale Gas Sediments. *J Can Pet Technol* **46** (10): 55–61. PETSOC-07-10-06. https://doi.org/10.2118/07-10-06.

Jiao, K., Yao, S., Liu, C. et al. 2014. The Characterization and Quantitative Analysis of Nanopores in Unconventional Gas Reservoirs Utilizing FESEM–FIB and Image Processing: An Example from the Lower Silurian Longmaxi Shale, Upper Yangtze Region, China. *Int J Coal Geol* **128–129**: 1–11. https://doi.org/10.1016/j.coal.2014.03.004.

Jin, Z. and Firoozabadi, A. 2015a. Flow of Methane in Shale Nanopores at Low and High Pressure by Molecular Dynamics Simulations. *J Chem Phys* **143** (10). https://doi.org/10.1063/1.4930006.

Jin, Z. and Firoozabadi, A. 2015b. Phase Behavior and Flow in Shale Nanopores From Molecular Simulations. Paper presented at the SPE Annual Technical Conference and Exhibition, Houston, Texas, USA, 28–30 September. SPE-175151-MS. https://doi.org/10.2118/175151-MS.

Jones, J. E. 1924. On the Determination of Molecular Fields.—I. From the Variation of the Viscosity of a Gas with Temperature. *Proc R Soc Lond A Math Phys Sci* **106** (738): 441–462.

Kasaeian, A., Daneshazarian, R., Mahian, O. et al. 2017. Nanofluid Flow and Heat Transfer in Porous Media: A Review of the Latest Developments. *Int J Heat Mass Transf* **107**: 778–791. https://doi.org/10.1016/j.ijheatmasstransfer.2016.11.074.

Kondori, J., James, L., and Zendehboudi, S. 2019. Molecular Scale Modeling Approach to Evaluate Stability and Dissociation of Methane and Carbon Dioxide Hydrates. *J Mol Liq* **297**: 111503. https://doi.org/10.1016/j.molliq.2019.111503.

Kou, R., Alafnan, S. F. K., and Akkutlu, I. Y. 2017. Multi-Scale Analysis of Gas Transport Mechanisms in Kerogen. *Transp Porous Med* **116** (2): 493–519. https://doi.org/10.1007/s11242-016-0787-7.

Lee, T., Bocquet, L., and Coasne, B. 2016. Activated Desorption at Heterogeneous Interfaces and Long-Time Kinetics of Hydrocarbon Recovery from Nanoporous Media. *Nat Commun* **7** (1): 1–10. https://doi.org/10.1038/ncomms11890.

Liehui, Z., Baochao, S., Yulong, Z. et al. 2019. Review of Micro Seepage Mechanisms in Shale Gas Reservoirs. *Int J Heat Mass Transf* **139**: 144–179. https://doi.org/10.1016/j.ijheatmasstransfer.2019.04.141.

Lifson, S., Hagler, A. T., and Dauber, P. 1979. Consistent Force Field Studies of Intermolecular Forces in Hydrogen-Bonded Crystals. 1. Carboxylic Acids, Amides, and the C:O.Cntdot..Cntdot..Cntdot.H- Hydrogen Bonds. *J Am Chem Soc* **101** (18): 5111–5121. https://doi.org/10.1021/ja00512a001.

Li, S., Meng, F., Zhang, X. et al. 2021. Gas Composition and Carbon Isotopic Variation during Shale Gas Desorption: Implication from the Ordovician Wufeng Formation - Silurian Longmaxi Formation in West Hubei, China. *J Nat Gas Sci Eng* **87**: 103777. https://doi.org/10.1016/j.jngse.2020.103777.

Li, W., Nan, Y., Zhang, Z. et al. 2020. Hydrophilicity/Hydrophobicity Driven CO2 Solubility in Kaolinite Nanopores in Relation to Carbon Sequestration. *Chem Eng J* **398**: 125449. https://doi.org/10.1016/j.cej.2020.125449.

Liu, Y.-C., Wang, Q., and Li, X.-F. 2005. A Diffusion Model for the Fluids Confined in Micropores. *J Chem Phys* **122** (4): 044714. https://doi.org/10.1063/1.1839557.

Louk, K., Ripepi, N., Luxbacher, K. et al. 2017. Monitoring CO2 Storage and Enhanced Gas Recovery in Unconventional Shale Reservoirs: Results from the Morgan County, Tennessee Injection Test. *J Nat Gas Sci Eng* **45**: 11–25. https://doi.org/10.1016/j.jngse.2017.03.025.

Lu, T., Xu, R., Zhou, B. et al. 2019. Improved Method for Measuring the Permeability of Nanoporous Material and Its Application to Shale Matrix with Ultra-Low Permeability. *Materials (Basel)* **12** (9). https://doi.org/10.3390/ma12091567.

Malek, K. and Coppens, M.-O. 2003. Knudsen Self- and Fickian Diffusion in Rough Nanoporous Media. *J Chem Phys* **119** (5): 2801–2811. https://doi.org/10.1063/1.1584652.

MATLAB. 2020. MATLAB Software Version 9.9.0.1467703 (R2020b). Natick, Massachusetts: The MathWorks Inc.

Ma, J., Zhang, Z., Xiang, Y. et al. 2017. On the Prediction of Transport Properties of Ionic Liquid Using 1-n-Butylmethylpyridinium Tetrafluoroborate as an Example. *Mol Simul* **43** (18): 1502–1512. https://doi.org/10.1080/08927022.2017.1321760.

Miller, C. C. 1924. The Stokes-Einstein Law for Diffusion in Solution. *Proc R Soc Lond A Math Phys Sci* **106** (740): 724–749.

Mouas, M., Gasser, J.-G., Hellal, S. et al. 2012. Diffusion and Viscosity of Liquid Tin: Green-Kubo Relationship-Based Calculations from Molecular Dynamics Simulations. *J Chem Phys* **136** (9). https://doi.org/10.1063/1.3687243.

Nanok, T., Artrith, N., Pantu, P. et al. 2009. Structure and Dynamics of Water Confined in Single-Wall Nanotubes. *J Phys Chem A* **113** (10): 2103–2108. https://doi.org/10.1021/jp8088676.

Pang, Y., Soliman, M. Y., Deng, H. et al. 2017. Experimental and Analytical Investigation of Adsorption Effects on Shale Gas Transport in Organic Nanopores. *Fuel* **199**: 272–288. https://doi.org/10.1016/j.fuel.2017.02.072.

Phan, A., Ho, T. A., Cole, D. R. et al. 2012. Molecular Structure and Dynamics in Thin Water Films at Metal Oxide Surfaces: Magnesium, Aluminum, and Silicon Oxide Surfaces. *J Phys Chem C* **116** (30): 15962–15973. https://doi.org/10.1021/jp300679v.

Phillip, W. A., Rzayev, J., Hillmyer, M. A. et al. 2006. Gas and Water Liquid Transport through Nanoporous Block Copolymer Membranes. *J Membr Sci* **286** (1–2): 144–152. https://doi.org/10.1016/j.memsci.2006.09.028.

Rapaport, D. C. 2004. *The Art of Molecular Dynamics Simulation*. Cambridge, UK: Cambridge University Press. https://doi.org/10.1017/CBO9780511816581.

Rappe, A. K., Casewit, C. J., Colwell, K. S. et al. 1992. UFF, a Full Periodic Table Force Field for Molecular Mechanics and Molecular Dynamics Simulations. *J Am Chem Soc* **114** (25): 10024–10035. https://doi.org/10.1021/ja00051a040.

Ross, D. J. K. and Marc Bustin, R. 2009. The Importance of Shale Composition and Pore Structure upon Gas Storage Potential of Shale Gas Reservoirs. *Mar Pet Geol* **26** (6): 916–927. https://doi.org/10.1016/j.marpetgeo.2008.06.004.

Rudd, R. E. and Broughton, J. Q. 1998. Coarse-Grained Molecular Dynamics and the Atomic Limit of Finite Elements. *Phys Rev B* **58** (10): R5893–R5896. https://doi.org/10.1103/PhysRevB.58.R5893.

Severson, B. L. and Snurr, R. Q. 2007. Monte Carlo Simulation of N-Alkane Adsorption Isotherms in Carbon Slit Pores. *J Chem Phys* **126** (13): 134708. https://doi.org/10.1063/1.2713097.

Shen, Y., Pang, Y., Shen, Z. et al. 2018. Multiparameter Analysis of Gas Transport Phenomena in Shale Gas Reservoirs: Apparent Permeability Characterization. *Sci Rep* **8** (1): 1–14. https://doi.org/10.1038/s41598-018-20949-2.

Shilov, E., Dorhjie, D. B., Mukhina, E. et al. 2021. Experimental and Numerical Studies of Rich Gas Huff-n-Puff Injection in Tight Formation. *J Pet Sci Eng* **2**: 109420. https://doi.org/10.1016/j.petrol.2021.109420.

Singh, S. K., Sinha, A., Deo, G. et al. 2009. Vapor−Liquid Phase Coexistence, Critical Properties, and Surface Tension of Confined Alkanes. *J Phys Chem C* **113** (17): 7170–7180. https://doi.org/10.1021/jp8073915.

Skarmoutsos, I., Tamiolakis, G., and Froudakis, G. E. 2013. Carbon-Based Nanoporous Networks as Media for the Separation of CO_2/CH_4 Mixtures: A Molecular Dynamics Approach. *J Phys Chem C* **117** (38): 19373–19381. https://doi.org/10.1021/jp401978m.

Skoulidas, A. I. and Sholl, D. S. 2003. Molecular Dynamics Simulations of Self-Diffusivities, Corrected Diffusivities, and Transport Diffusivities of Light Gases in Four Silica Zeolites To Assess Influences of Pore Shape and Connectivity. *J Phys Chem A* **107** (47): 10132–10141. https://doi.org/10.1021/jp0354301.

Skoulidas, A. I., Ackerman, D. M., Johnson, J. K. et al. 2002. Rapid Transport of Gases in Carbon Nanotubes. *Phys Rev Lett* **89** (18). https://doi.org/10.1103/PhysRevLett.89.185901.

Sobolewski, E., Makowski, M., Oldziej, S. et al. 2009. Towards Temperature-Dependent Coarse-Grained Potentials of Side-Chain Interactions for Protein Folding Simulations. I: Molecular Dynamics Study of a Pair of Methane Molecules in Water at Various Temperatures. *Protein Eng Des Sel* **22** (9): 547–552. https://doi.org/10.1093/protein/gzp028.

Song, H., Yu, M., Zhu, W. et al. 2015. Numerical Investigation of Gas Flow Rate in Shale Gas Reservoirs with Nanoporous Media. *Int J Heat Mass Transf* **80**: 626–635. https://doi.org/10.1016/j.ijheatmasstransfer.2014.09.039.

Striolo, A., Chialvo, A. A., Cummings, P. T. et al. 2003. Water Adsorption in Carbon-Slit Nanopores. *Langmuir* **19** (20): 8583–8591. https://doi.org/10.1021/la0347354.

Stukowski, A. 2009. Visualization and Analysis of Atomistic Simulation Data with OVITO–the Open Visualization Tool. *Modelling Simul Mater Sci Eng* **18** (1): 015012. https://doi.org/10.1088/0965-0393/18/1/015012.

Talu, O. and Myers, A. L. 2001. Reference Potentials for Adsorption of Helium, Argon, Methane, and Krypton in High-Silica Zeolites. *Colloids Surf A Physicochem Eng Asp* **187–188**: 83–93. https://doi.org/10.1016/S0927-7757(01)00628-8.

Tesson, S. and Firoozabadi, A. 2018. Methane Adsorption and Self-Diffusion in Shale Kerogen and Slit Nanopores by Molecular Simulations. *J Phys Chem C* **122** (41): 23528–23542. https://doi.org/10.1021/acs.jpcc.8b07123.

Thompson, A. P., Aktulga, H. M., and Berger, R. 2022. LAMMPS - a Flexible Simulation Tool for Particle-Based Materials Modeling at the Atomic, Meso, and Continuum Scales. *Comput Phys Commun* **271**. https://doi.org/10.1016/j.cpc.2021.108171.

Wei, G., Xiong, W., Shusheng, G. et al. 2013. Impact of Temperature on the Isothermal Adsorption/Desorption of Shale Gas. *Pet Explor Dev* **40** (4): 514–519. https://doi.org/10.1016/S1876-3804(13)60066-X.

Wu, K., Chen, Z., and Li, X. 2015a. Real Gas Transport through Nanopores of Varying Cross-Section Type and Shape in Shale Gas Reservoirs. *Chem Eng J* **281**: 813–825. https://doi.org/10.1016/j.cej.2015.07.012.

Wu, K., Li, X., Wang, C. et al. 2015b. A Model for Surface Diffusion of Adsorbed Gas in Nanopores of Shale Gas Reservoirs. Paper presented at the Offshore Technology Conference, Houston, Texas, USA, 4–7 May. OTC-25662-MS. https://doi.org/10.4043/25662-MS.

Xiang, L. and Elsworth, D. 2015. Geomechanics of CO_2 Enhanced Shale Gas Recovery. *J Nat Gas Sci Eng* **26**: 1607–1619. https://doi.org/10.1016/j.jngse.2014.08.010.

Xu, R., Zeng, K., Zhang, C. et al. 2017. Assessing the Feasibility and CO_2 Storage Capacity of CO_2 Enhanced Shale Gas Recovery Using Triple-Porosity Reservoir Model. *Appl Therm Eng* **115**: 1306–1314. https://doi.org/10.1016/j.applthermaleng.2017.01.062.

Yamashita, K., Kashiwagi, K., Agrawal, A. et al. 2017. Grand Canonical Monte Carlo and Molecular Dynamics Simulations of Capillary Condensation and Evaporation of Water in Hydrophilic Mesopores. *Mol Phys* **115** (3): 328–342. https://doi.org/10.1080/00268976.2016.1262555.

Yan, Y., Dong, Z., Zhang, Y. et al. 2017. CO_2 Activating Hydrocarbon Transport across Nanopore Throat: Insights from Molecular Dynamics Simulation. *Phys Chem Chem Phys* **19** (45): 30439–30444. https://doi.org/10.1039/c7cp05759h.

Yu, S., Bo, J., and Jie-gang, L. 2017. Nanopore Structural Characteristics and Their Impact on Methane Adsorption and Diffusion in Low to Medium Tectonically Deformed Coals: Case Study in the Huaibei Coal Field. *Energy Fuels* **31** (7): 6711–6723. https://doi.org/10.1021/acs.energyfuels.7b00512.

Zhang, P., Hu, L., Meegoda, J. N. et al. 2015. Micro/Nano-Pore Network Analysis of Gas Flow in Shale Matrix. *Sci Rep* **5** (1): 1–11. https://doi.org/10.1038/srep13501.